Received: 13 May 2023 | Revised: 13 July 2023 | Accepted: 25 July 2023

DOI: 10.1111/clr.14157

ORIGINAL ARTICLE

CLINICAL ORAL IMPLANTS RESEARCH WILEY

Influence of straight versus angulated screw channel titanium bases on failure loads of two-piece ceramic and titanium implants restored with screw-retained monolithic crowns: An in-vitro study

E. Helal[1] | P. C. Gierthmuehlen[1] | E. A. Bonfante[2] | T. M. B. Campos[2] | L. S. Prott[1] | R. Langner[3,4] | F. A. Spitznagel[1]

[1]Department of Prosthodontics, Medical Faculty and University Hospital Düsseldorf, Heinrich-Heine-University Düsseldorf, Düsseldorf, Germany

[2]Department of Prosthodontics and Periodontology, Bauru School of Dentistry, University of Sao Paulo, Bauru, Brazil

[3]Institute of Systems Neuroscience, Medical Faculty, Heinrich-Heine-University Düsseldorf, Düsseldorf, Germany

[4]Institute of Neuroscience and Medicine, Brain and Behavior (INM-7), Research Center Jülich, Jülich, Germany

Correspondence
F. A. Spitznagel, Department of Prosthodontics, Medical Faculty and University Hospital Düsseldorf, Heinrich-Heine-University, Moorenstraße 5, 40225 Düsseldorf, Germany.
Email: frank.spitznagel@med.uni-duesseldorf.de

Abstract

Objective: To analyze the influence of titanium-base (straight [SSC]/angulated-screw-channel [ASC]) on failure-loads and bending-moments of two-piece ceramic and titanium–zirconium implants restored with monolithic-zirconia crowns after fatigue.

Materials and Methods: Thirty-two anterior monolithic-screw-retained zirconia crowns were divided into four groups ($n = 8$/group) according to the factors: (1) type of implant material: two-piece titanium–zirconium implant (Ti–Zr; control-group) versus two-piece ceramic implant (CI; test-group) and (2) type of titanium-base: SSC (0° angle) versus ASC (25°). An intact implant was used for field emission gun-scanning electronic microscopy (FEG-SEM) characterization and Raman spectroscopy for phase analyses and residual stress quantification. All samples were exposed to fatigue with thermodynamic loading (1.2-million-cycles, 49 N, 1.6 Hz, 5–55°C) at a 30° angle. Surviving specimens were loaded until failure (SLF) and bending moments were recorded. Failed samples were examined using light microscope and SEM. Statistical analyses included ANOVA and Mann–Whitney *U*-test.

Results: Raman-spectroscopy revealed the presence of residual compressive stresses. FEG-SEM revealed a roughened surface between threads and polished surface at the cervical-collar of the ceramic implant. All samples survived fatigue and were free of complications. Mean bending-moments (±SD) were: Ti-Zr-0: 241 ± 45 N cm, Ti-Zr-25: 303 ± 86 N cm, CI-0: 326 ± 58 N cm, CI-25: 434 ± 71 N cm. Titanium-base and implant-material had significant effects in favor of ASC titanium bases ($p = .001$) and ceramic-implants ($p < .001$). Failure analysis after SLF revealed severe fractures in ceramic implants, whereas titanium implants were restricted to plastic deformation.

Conclusions: Ceramic and titanium implants exhibited high reliability after fatigue, with no failures. From a mechanical perspective, titanium bases with ASC can be recommended for both ceramic and titanium implants and are safe for clinical application.

KEYWORDS
aging, ceramics, dental implant, fatigue, material testing, zirconia

1 | INTRODUCTION

In the quest for a suitable tooth-colored and non-metallic alternative to the gold-standard of titanium dental implants, ceramic implants made of alumina-toughened zirconia (ATZ) or 3 mol% yttria-doped tetragonal zirconia (Y-TZP) have evolved (Balmer et al., 2022; Cionca et al., 2017). Ceramic implants might serve especially in the esthetic zone as a valuable treatment addendum for dental implantology owing to their appealing esthetic outcome and tooth-like color (Kniha et al., 2019). Experimental studies have confirmed equivalent osseointegration processes, bone-to-implant contact, and soft tissue healing for ceramic and titanium implants in both, preclinical and clinical investigations (Bienz et al., 2021; Roehling et al., 2019; Thoma et al., 2015). Clinical trials and systematic reviews have reported high mid-term survival rates of 94.3%–97.7% after 5 years of observation for ceramic implants (Gahlert et al., 2022; Kohal et al., 2020; Spitznagel et al., 2022).

To date, most studies have primarily investigated one-piece ceramic implants with good mechanical stability and high fracture resistance (Balmer et al., 2022; Bethke et al., 2020). However, a significant disadvantage of one-piece ceramic implants is limited prosthetic versatility and lack of compensation for abutment angulation (Balmer et al., 2022). Consequently, two-piece ceramic implants have been developed, first with an adhesive joint and then with a screw-retained connection (Janner et al., 2018; Spies et al., 2016). One of the first clinical trials reported a 100% survival rate after 15 months of functional loading for screw-retained restorations supported by a novel two-piece ceramic implant (Lorenz et al., 2022).

The esthetic zone of the maxilla presents a great clinical challenge for predictable functional and esthetic long-term success in implant dentistry (Buser et al., 2004; Chen et al., 2023). Therefore, the correct three-dimensional implant position according to the prosthetic plan is paramount to prevent complications and adverse esthetic outcomes (Chen et al., 2023).

Considering recent recommendations regarding the retention of implant-supported single crowns, screw-retained reconstructions are favored over cement-retained restorations to prevent the risk of peri-implant infections with possible residual cement surpluses (Sailer et al., 2022; Staubli et al., 2017; Wilson Jr., 2009). However, anatomical variations with undercuts, post-extraction ridge alterations, insufficient bone volume, and natural angulation of the maxillary teeth hamper palatal positioning of the screw-access hole and axial loading of the implant (Chappuis et al., 2013; Pitman et al., 2022).

To overcome poor esthetic results due to an access hole on the vestibular surface, the concept of angulated screw channels (ASCs) for titanium implants was introduced in 2015 (Garcia-Gazaui et al., 2015; Pitman et al., 2022; Rella et al., 2021). Depending on the system, ASCs allow an axis correction of up to 25° and shift of the screw-access hole to the more favorable palatal position (Edmondson et al., 2022; Rella et al., 2021). A recent cone-beam computed tomography study compared the prevalence of screw-retained reconstructions with straight versus angulated abutments in the anterior maxilla (Edmondson et al., 2022). Angulated abutments with an average axis compensation of 15° were enabled in 76% cases of screw-retained reconstruction, whereas only 24% could be enabled with a straight abutment (Edmondson et al., 2022).

Despite meeting esthetic demands, technical complications such as chipping of the veneering ceramic, abutment fracture, and screw loosening and fracture remain with angulated abutment solutions.

Recent evidence suggests that angulated abutments might be associated with higher mechanical complications due to off-axis loading and inferior preload on the abutment screw; this may result in premature screw loosening, followed by fracture and restoration failure (Hein et al., 2021; Hotinski & Dudley, 2019; Opler et al., 2020). However, clinical trials have reported high survival rates of 92%–96% for ASC reconstructions on titanium implants up to 3 years, with only a few technical complications (Di Fiore et al., 2023; Lv et al., 2021; Rella et al., 2021).

To the best of our knowledge, there is currently no study which investigates ASC implant crowns for two-piece ceramic implants, compared to that of titanium implants from a mechanical perspective in the esthetic zone. Therefore, this topic needs to be elucidated.

Fatigue testing under cyclic loads is an accepted method for estimating the lifetime and failure mode of implant-supported reconstructions (Bonfante & Coelho, 2016).

Therefore, the aim of the present laboratory study was to test whether screw-retained titanium bases (straight screw channel [SSC] vs. ASC) affect failure load and bending moments of two-piece zirconia implants, compared to those of two-piece titanium implants. The tested null hypotheses suggested that the type of (i) titanium base (SSC vs. ASC) and (ii) implant material (ceramic vs. titanium) do not influence the failure load and bending moments of screw-retained anterior monolithic zirconia crowns after fatigue.

2 | MATERIALS AND METHODS

2.1 | Study design

A total of 32 occlusal screw-retained monolithic translucent multilayer zirconia crowns (Katana UTML, Kuraray Noritake) were either supported by a two-piece ceramic implant system (PURE Ceramic Implant [CI] 4.1×12 mm, ZLA; Straumann) as test groups or a two-piece titanium–zirconium alloy implant system (Standard Plus 4.1×12 mm, Roxolid, SLA; Straumann) serving as control. The two groups were further divided into two subgroups ($n=8$ each) according to their respective titanium bases (SSC vs. ASC) (Figures 1 and 2).

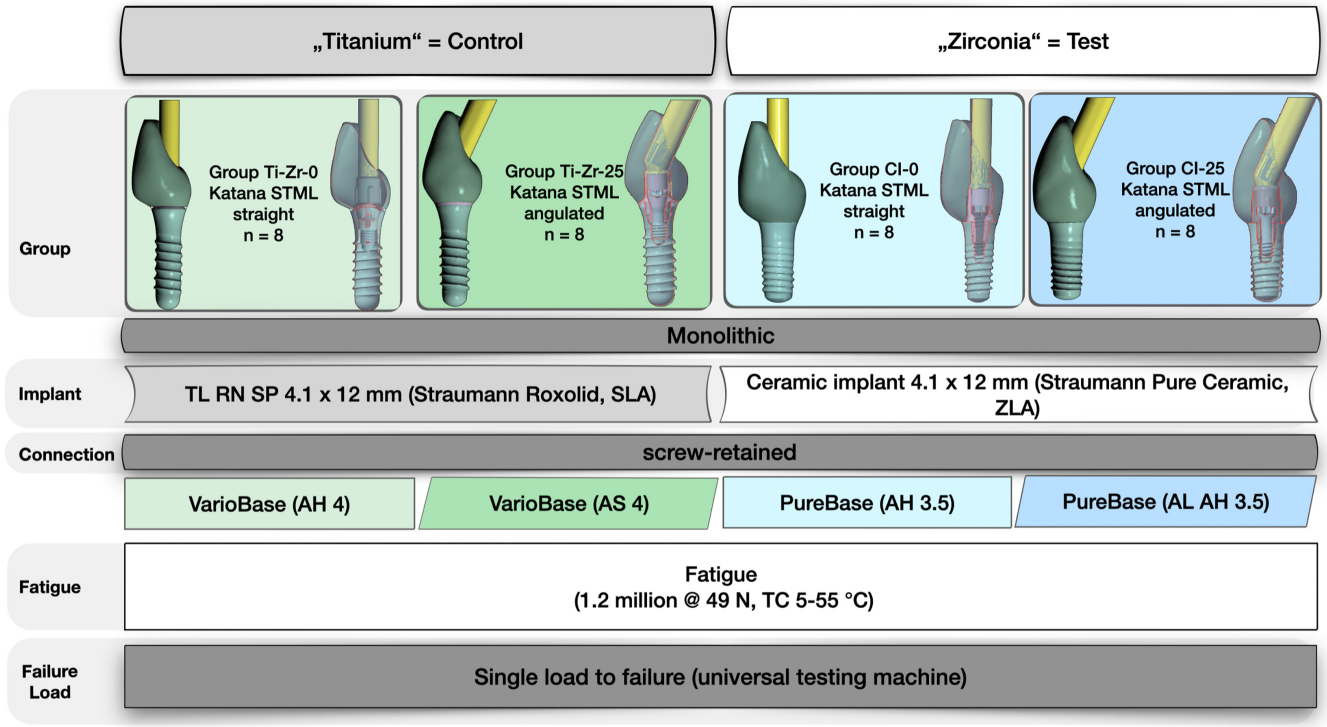

FIGURE 1 Experimental test setup.

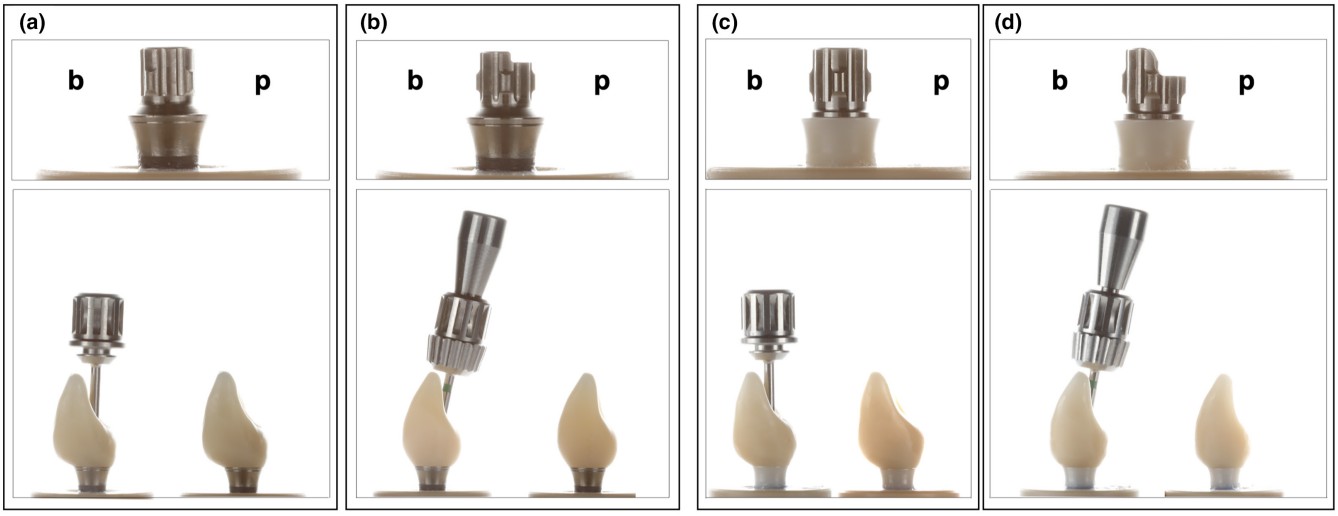

FIGURE 2 Overview of different test groups with respective titanium bases and anterior monolithic zirconia crowns (b: buccal, p: palatal): (a) Group Ti-Zr-0, (b) Group Ti-Zr-25, (c) Group CI-0, (d) Group CI-25.

Group Ti-Zr-0 (control): A two-piece titanium–zirconium implant with a SSC titanium base (RN Variobase, AH 4 mm, Straumann).

Group Ti-Zr-25 (test): A two-piece titanium–zirconium implant with an ASC titanium base (RN Variobase AS, AH 4 mm, Straumann).

Group CI-0 (test): A two-piece zirconia implant with a SSC titanium base (CI RD PURE Base, AH 3.5 mm, Straumann).

Group CI-25 (test): A two-piece zirconia implant with an ASC titanium base (CI RD PURE Base, AL 3.5 mm, Straumann).

2.2 | Ceramic implant characterization

The microstructure of a pristine ceramic implant was analyzed using a field-emission gun scanning electron microscope (FEG-SEM; MIRA3-TESCAN). SEM micrographs were obtained using secondary (SE) and backscattered (BSE) electron detectors, at high vacuum, 5 kV accelerating voltage, and magnifications from 10,000 to 100,000×. Two regions of interest were evaluated: the cervical collar and the region between threaded areas.

Residual stress was measured using Raman spectroscopy. The specimens were fixed to a specially designed compressive loading device and placed on a confocal Raman spectrometer (LabRAM HR Evolution). The spectra were recorded between 520 and 700 cm^{-1}, slit size of 100 µm, with an acquisition time of 30 s and 2 cycles. Residual compressive stress was determined according to the following equation (Tanaka et al., 2009).

$$\nu = \nu_0 + \Pi\Delta\sigma$$

where ν is the Raman peak position shift of the aged specimen, ν_0 is the Raman peak position of the immediate sample, and Π is the coefficient for uniaxial stress (constant = 5.43 $cm^{-1}GPa^{-1}$).

2.3 | Fabrication of specimens

All implants were embedded perpendicularly in a dual-curing composite (LuxaCore Z Dual, DMG), with a modulus of elasticity of 9.3 GPa in polyether ether ketone (PEEK) tubes. To mimic reported clinical conditions with marginal bone losses of 0.7 mm after 1 year and 0.99 mm after 5 years for zirconia implants, a bony recession of 0.5–1 mm between the implant neck and the resin surface was set (Gahlert et al., 2022; Pieralli et al., 2017; Roehling et al., 2018).

2.4 | Fabrication of implant restorations

The study design simulated the replacement of a central incisor in the esthetic zone. For standardization, one implant in each subgroup was embedded in the prosthetically correct position (Group Ti-Zr-0 and CI-0) at the location of the maxillary central incisor (FDI 21) or at a 25° deviation from this position (Group Ti-Zr-25 and CI-25) for screw-retained restoration in a master model (Frasaco-Model). Subsequently, a scan body (Ti-Zr: Cares RN Mono-Scan body and CI: Cares CI RD Mono-Scan body, Straumann) was screwed into the respective implant, and a digital impression (Trios3, 3Shape) was obtained. A standardized central incisor was designed in a CAD-software (Ceramill Mind V3.0-7783, Amann Girrbach). A master design was used for all monolithic crowns to produce identical and comparable test samples for each subgroup. Implant crowns were milled in a five-axis milling machine (Ceramill Motion 2, Amann Girrbach) out of a 5Y-TZP multilayer zirconia disc (Katana UTML, Kuraray Noritake) with a flexural strength of 557 MPa (according to the manufacturer), followed by sintering and glazing (Cerabien ZR Clear Glaze, Kuraray Noritake). All implant restorations were produced by one experienced dental technician, according to the manufacturer's recommendations. Prior to adhesive bonding, the inner surfaces of the zirconia crowns were air abraded with 50 µm aluminum oxide at a pressure of 2 bar. Subsequently, the implant crowns and their corresponding titanium bases were conditioned with a 10-methacryloyloxydecyl dihydrogen phosphate (MDP) primer (Clearfil Ceramic Primer Plus, Kuraray Noritake) and resin-bonded with a self-curing composite cement (Panavia V5 opaque, Kuraray Noritake).

Both straight and angulated monolithic zirconia crowns were tightened to their corresponding implants at 35 N cm using a torque control (Ratchet and Torque Control Device, Straumann), and retightened after 10 min to prevent screw loosening (Farina et al., 2014; Spazzin et al., 2010). The screw access holes were filled with Teflon tape (Kirchhoff GmbH) and closed using a resin composite (Tetric Evo Ceram A2, Ivoclar).

2.5 | Fatigue analysis

All specimens were subjected to cyclic mechanical loading (1.2 million cycles, 49 N, 1.6 Hz) with simultaneous thermocycling (5–55°C, dwell time 120 s) in a chewing simulator (CS-4.8 professional line, SD Mechatronik). The specimens were loaded 2 mm below the incisal edge on the palatal surface at a 30° angle using a steatite ball antagonist ($r = 3$ mm; Hoechst Ceram Tec) adapted from ISO 14801 (Cantarella et al., 2021; ISO14801, 2016). The vertical movement during each chewing cycle was 2 mm. During loading, the specimens were regularly examined for cracks, fractures/failures, or mobility of the implant-reconstruction complex (screw loosening/debonding). The survival rate after fatigue was calculated based on complications, which were divided into non-serious events (e.g., cracks and screw loosening) and serious failures (e.g., fractures).

2.6 | Single load to failure

All samples were loaded until failure (crosshead speed of 1.5 mm min^{-1}) in a universal testing machine (Zwick Z010/TN2S, Zwick Roell). Load was applied to the palatal surface of the implant restoration at an angle of 30°, as during fatigue (ISO14801, 2016). To avoid force peaks and guarantee an even force distribution during static loading, a tin foil of 0.5 mm thickness (Dentaurum) was placed between the specimens and the load indenter (stainless steel ball with 6 mm diameter) (Cantarella et al., 2021). Failure was defined as either a visible crack or fracture of the implant-restoration complex, or a 20% decrease in the maximum load (F_{max}) without an obvious fracture. Apart from load to failure (N), bending moments (M) were individually calculated for each sample in N cm according to the formula $M = 0.5 \times F \times l$, wherein variable "$F$" and the lever arm "l" correspond to the maximum load (N) and the vertical distance from the simulated bone level to the center of load (cm), respectively (Cantarella et al., 2021).

2.7 | Failure and Fractographic analysis

Failure analyses were performed after fatigue and single load-to-failure testing using a polarized light microscope (Zeiss Axiocam 208 color, Carl Zeiss Microscopy). To improve the depth of focus, Z-stack mode (ZEN Core 3.3, Carl Zeiss Microscopy) was used to

capture several images with varying depths and stitch planes within the same image. Hereafter, the most representative samples were analyzed by SEM (Vega 3, Tescan) to further assess the mode and origin of failure.

2.8 | Statistical analysis

Power calculation (G*Power 3.1.9.2) provided an estimated power of >80% using eight samples per group, assuming any effect of at least large size (Cohen's effect size of $f > 0.4$) with respect to statistical testing using analysis of variance (ANOVA) and a two-sided type-I-error threshold of $p < .05$ for the two factors: (i) type of titanium base (SSC vs. ASC) and (ii) choice of implant material (titanium vs. ceramic) and their interactions.

Data were analyzed using the statistical software SPSS 26 (IBM Corp.). Levene's test was applied to test for homogeneity of error variance before using ANOVA for main effects and interactions of the two factors of interest (type of titanium base and implant material), followed by Mann–Whitney *U*-test for pairwise comparison of titanium base and implant material. The level of significance was defined as $p < .05$ (95% confidence interval [CI]) for all tests; data were visualized as boxplots.

3 | RESULTS

3.1 | Ceramic implant characterization

Figure 3 presents the FEG-SEM micrographs of the zirconia implant at both the cervical collar (Figure 3a–c) as well as in between the threads (d–f), with magnifications ranging from 10,000 to 100,000×. The magnified images (Figure 3b,c) show apparent polishing marks. Micrographs d, e, and f depict a roughened surface with shallow valleys. Under higher magnification (f), some particles encrusted over the zirconia surface can be observed.

Figure 4 depicts the Raman spectra of the zirconia implant in the cervical collar and regions between the threads. Bands corresponding to tetragonal or cubic zirconia were observed at both spots. The presence of monoclinic zirconia with defined peaks, that were not very intense, could be detected in both regions. A relevant finding is the dislodgement of band 634 cm^{-1} (Figure 4) suggesting the presence of residual compressive stresses, which can be calculated by the amount of dislodgement by the following formula: $\Delta\nu = \prod\Delta\sigma$ (Prado et al., 2020; Tanaka et al., 2009), wherein $\Delta\nu$ = band dislodgement, $\prod$ = (constant = 5.43 cm^{-1} GPa^{-1}) and $\Delta\sigma$ = variation in tensile stress. Based on these calculations, a value of −450 MPa was obtained.

3.2 | Dynamic loading

All samples survived the dynamic loading test, suggesting a simulated 5-year survival rate of 100% for all tested groups. Fracture of the implant or restoration, screw loosening, or debonding of the implant crown from the titanium base was not observed in any sample. All samples were free of serious or non-serious complications.

3.3 | Single load to failure

Failure loads varied from 226–681 N for titanium implants to 340–889 N for ceramic implants (Table 1). Bending moments for titanium implants were in the range of 138–444 N cm and for ceramic implants in the range of 235–598 N cm, respectively (Table 1; Figures 5 and 6).

The type of titanium base (SSC vs. ASC) and implant material (titanium vs. ceramic) had significant effects on failure load [titanium base: $F(1,28) = 14.45$, $p = .001$; implant material: $F(1,28) = 15.94$, $p < .001$] and bending moment [titanium base: $F(1,28) = 12.99$, $p = .001$; implant material: $F(1,28) = 20.81$, $p < 0.001$]. A significant interaction between the two factors (type of titanium base and implant material) for either failure load [$F(1,28) = 0.36$, $p = .552$] or bending moments [$F(1,28) = 1.00$, $p = 0.327$] was missing.

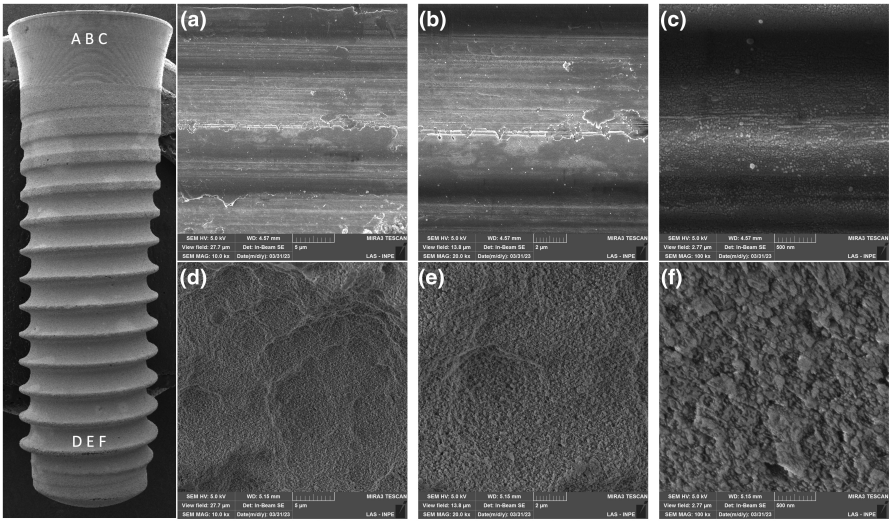

FIGURE 3 FEG-SEM micrographs showing an overview of the zirconia implant (left side) and increasing magnifications of the cervical collar (a, b, and c) and the area between the threads (d, e, and f). A polished surface is depicted at the cervical collar. A roughened surface is evident in the regions between the threads.

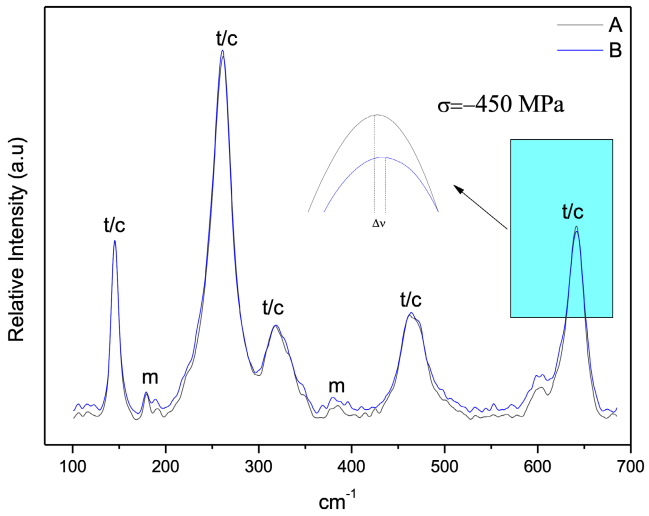

FIGURE 4 Raman spectra of the zirconia implant cervical collar (a) and the region between the threads (b); m, monoclinic zirconia; t/c, tetragonal or cubic zirconia.

TABLE 1 Descriptive statistics of failure load (mean ± standard deviation) and bending moment (mean ± standard deviation) of titanium–zirconium and ceramic implants with straight and angulated screw channel titanium bases.

Group	Load (N)	Bending moment (N cm)
Ti-Zr-0	360 ± 64	241 ± 45
Ti-Zr-25	473 ± 131	303 ± 86
CI-0	480 ± 83	326 ± 58
CI-25	635 ± 108	434 ± 71

The highest mean failure loads and bending moments were reported for Group CI-25 (635 ± 108 N, 434 ± 71 N cm), followed by groups CI-0 (480 ± 83 N, 326 ± 58 N cm), Ti-Zr-25 (473 ± 131 N, 303 ± 86 N cm), and Ti-Zr-0 (360 ± 64 N, 241 ± 45 N cm) (Table 1; Figures 5 and 6).

Post-hoc Mann–Whitney *U* tests revealed significant differences in failure load and bending moment in favor of ASC (vs. SSC) titanium bases for both titanium (failure load: $U = 10.0$, $p = .021$; bending moment: $U = 11.0$, $p = .028$) and ceramic implants (failure load and bending moment: $U = 6.0$, $p = .005$). Comparison of the implant materials separately for each type of titanium base revealed significant differences in the failure load and bending moment in favor of ceramic (vs. titanium) implants for both, straight (failure load: $U = 8.0$, $p = .01$; bending moment: $U = 9.0$, $p = .015$) and ASC titanium bases (failure load and bending moment: $U = 7$, $p = .007$).

3.4 | Failure modes and Fractographic analysis

Failure modes were subdivided into crown, abutment, and implant failures based on the level and origin of complications (Table 2).

Group CI specimens showed severe fracture failures at the implant level, with a higher incidence in ASC titanium bases (100%) than the straight ones (50%). The two main modes of failure at the implant level were as follows: a horizontal fracture just below the level of the embedding material and below the apical tip of the abutment screw or a combination of the former and an additional longitudinal fracture of the implant neck up to the horizontal fracture line (Figure 7). Half of the specimens (50%) in group CI-0 showed plastic deformation at the abutment level with a clear bend at the loading site, leading to failure (Figure 8). Failures at the crown level were not observed in either of the CI groups.

Samples from both Ti–Zr groups did not fracture catastrophically at the crown, abutment, or implant levels; however, they showed a slight plastic and ductile deformation at the abutment and implant levels, leading to failure (Table 2). Representative SEM micrographs of the fractured samples in both, SSC and ASC zirconia implant groups, showed several hackle lines, suggesting a centrifugal direction of crack propagation and fracture originating at the implant–abutment interface. Twist hackles were observed at the margin of the implant, and compression curls indicated fracture origin on the opposite side (Figures 9 and 10).

4 | DISCUSSION

The present in-vitro study analyzed the influence of SSC and ASC titanium bases on the failure load and bending moments of two-piece ceramic and titanium–zirconium implants after fatigue. The tested null hypotheses were rejected because the titanium base and implant material had significant effects on failure load and bending moment.

The microstructural appearance of the ceramic implant revealed by FEG-SEM images of regions between the threads resembles a sandblasted and acid-etched surface with the aim to increase roughness (Ramos et al., 2019) to eventually improve osseointegration parameters (Nishihara et al., 2019). Airborne particle abrasion methods can lead to occurrence of compressive residual stresses, as quantified by the Raman spectra. Similar findings have been reported previously by studies wherein sandblasting was performed on alumina alloys leading to the occurrence of compressive residual stresses (Righetti et al., 2020). Grain contours and typical zirconia microstructures were not observed in the micrographs of the zirconia implant cervical collar, where a machined surface appeared, as previously shown (Alves et al., 2022).

All specimens survived cyclic mechanical loading with simultaneous thermocycling and were free of serious and non-serious complications. The applied fatigue testing protocol with 1.2 million chewing cycles simulates mid-term aging equivalent to 5 years of clinical observation (Delong et al., 1985; Kern et al., 1999; Rosentritt et al., 2009). Although this test protocol does not simulate long-term behavior (for 10–40 years), it can predict potential early mechanical failures and is a well-accepted method that has been used in

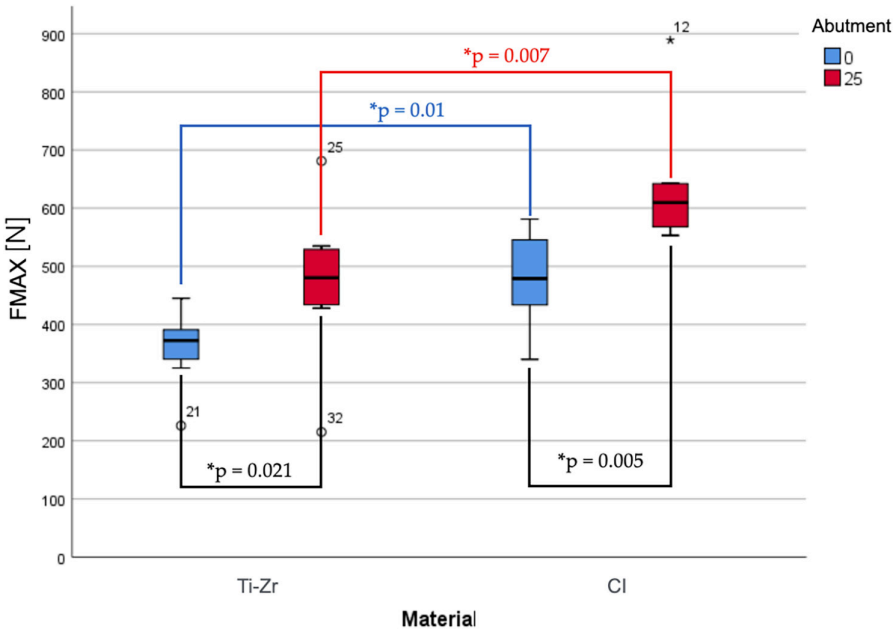

FIGURE 5 Boxplot of failure loads (F_{max} in N). Asterisk indicates statistical significance ($p < .05$).

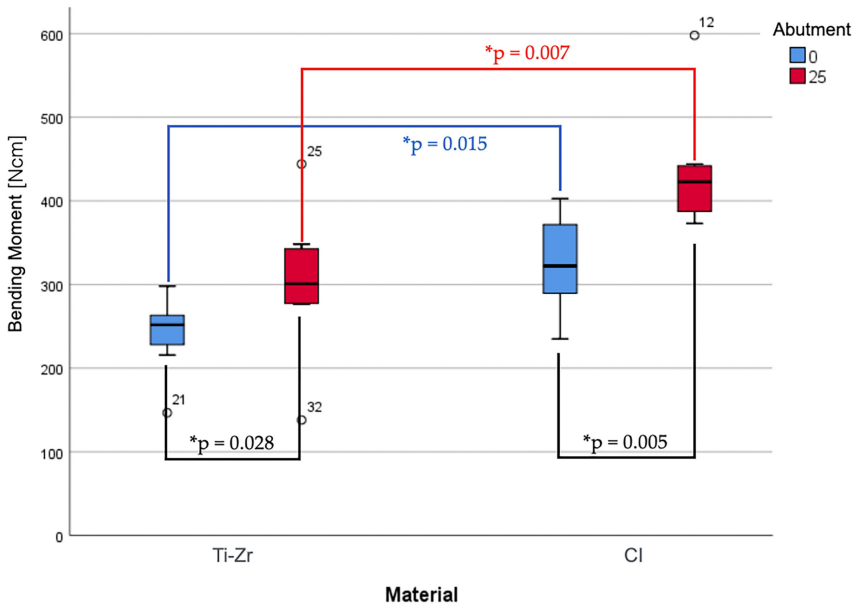

FIGURE 6 Boxplot of bending moments (in N cm). Asterisk indicates statistical significance ($p < .05$).

comparable studies (Cantarella et al., 2021; Joos et al., 2020). The test setup with dynamic loading and simultaneous thermocycling imitated a hostile oral environment to the best possible extent. The load during chewing simulation was applied at an angle of 30° to the vertical axis, as recommended by ISO 14801 (2016). To mimic a more clinically relevant scenario, the embedding procedure, restoration with anatomical crowns instead of loading hemispheres, differed from that of ISO 14801 (2016). The simulated bony recession of 0.5–1 mm does not correspond to the worst case scenario of 3 mm as described by ISO 14801; however, it is closer to clinical reality with reported marginal bone losses of 0.7–0.99 mm after up to 5 years of follow-up for ceramic implants (Gahlert et al., 2022; Pieralli et al., 2017; Roehling et al., 2018). To add to the stress on the implant-restoration complex, horizontal shear forces and an aqueous environment were applied, although this is not demanded by the ISO standard (Zhang et al., 2020). Studies are difficult or impossible to compare unless bending moments or individual lever arms to calculate bending moments are reported in addition to failure loads on deviation from the ISO standard (Bethke et al., 2020).

The investigated two-piece ceramic implant is a cylindrical screw-type Y-TZP soft tissue level zirconia implant with an endosteal diameter of 4.1 mm, a 1.8 mm machined collar with a 4.8 diameter, and an internal connection with a rotational lock (Janner et al., 2018). The corresponding titanium base is narrow, with a diameter smaller than that of the implant platform, which enables contact of the implant crown with the surrounding soft tissue (Lorenz et al., 2022). The titanium base has two heights—short (3.5 mm for CI and 4 mm for Ti-Zr) and long (5.5 mm for CI and 6 mm for Ti-Zr).

Group	Crown fracture	Abutment fracture	Abutment deformation	Implant fracture	Implant deformation
Ti-Zr-0	0% (0/8)	0% (0/8)	100% (8/8)	0% (0/8)	100% (8/8)
Ti-Zr-25	0% (0/8)	0% (0/8)	100% (8/8)	0% (0/8)	100% (8/8)
CI-0	0% (0/8)	0% (0/8)	50% (4/8)	50% (4/8)	0% (0/8)
CI-25	0% (0/8)	0% (0/8)	0% (0/8)	100% (8/8)	0% (0/8)

TABLE 2 Overview of failure modes after single load-to-failure testing.

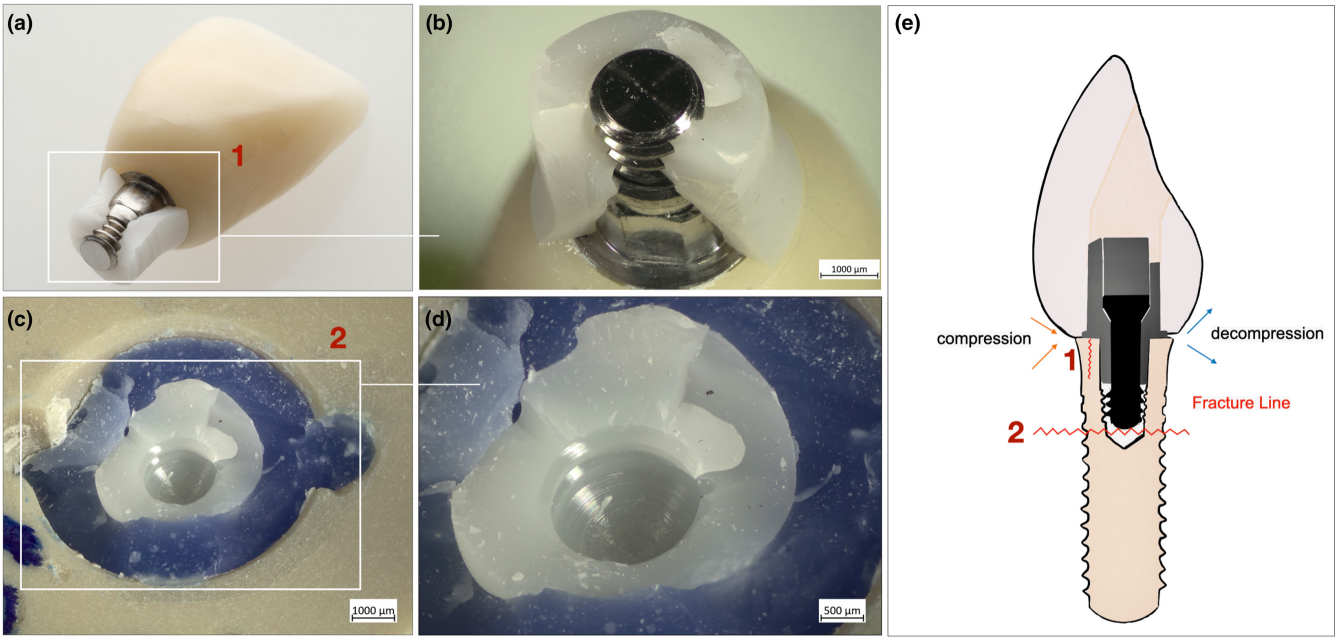

FIGURE 7 Characteristic failed sample of group CI-25 with implant fracture. (a) longitudinal implant fracture and (b) detailed view. (c) Horizontal implant fracture and (d) detailed view. (e) Schematic illustration of main fracture modes.

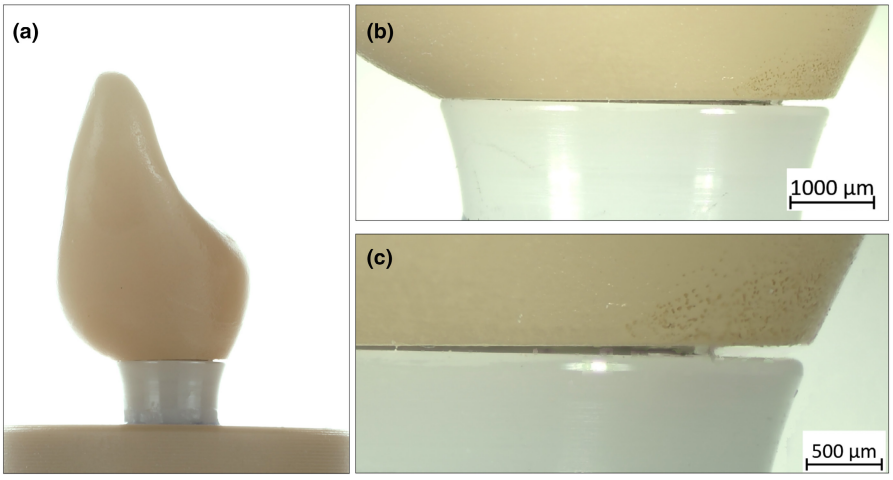

FIGURE 8 Characteristic failed sample of group CI-0 with titanium base deformation. (a) Overview. (b) and (c) detailed view with pronounced bend up on the loading site (flexion) leading to failure.

As a shorter titanium base was used in this study for both the SSC and ASC samples, it can be concluded that a longer abutment height can lead to higher failure loads and bending moments. The rationale for using a short rather than a long abutment height was to further simulate a possible worst-case scenario with an unfavorable loading condition (Zhang, Yu, & Yu, 2022). Finite element analysis studies on titanium implants have shown that angulation and deviation from an ideal central implant position to the buccal side could affect stress distribution, leading to increased mechanical strain on the implant and restorative components, especially the prosthetic screw, titanium base neck, and upper cortical bone (Korkmaz & Kul, 2022; Zhang, Yu, & Yu, 2022).

In the present investigation, mean failure load values and respective bending moments ranged for Ti–Zr groups from 360–473 N and 241–303 N cm, and for CI groups from 480–635 N and 326–434 N cm. A comparable study reported failure loads of 942 N for

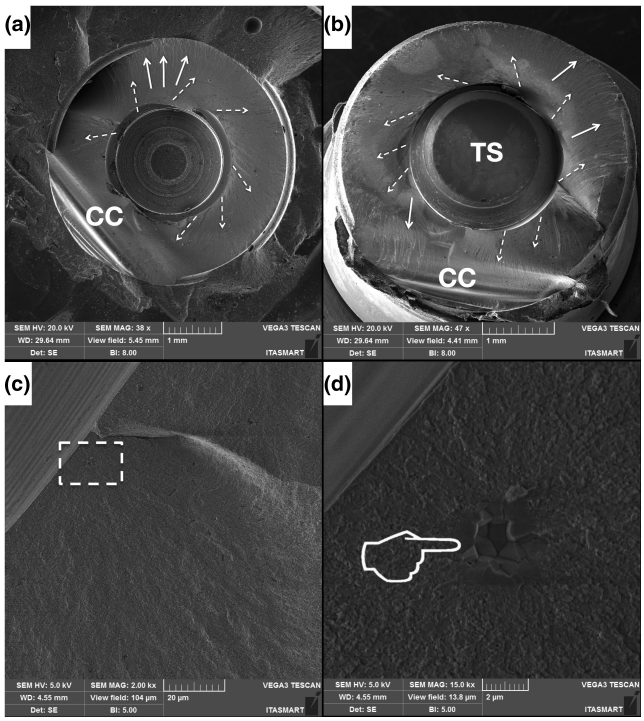

FIGURE 9 Representative SEM micrographs of fractured sample of two-piece zirconia implant with a straight titanium base (Group CI-0). (a) Occlusal view of the zirconia implant with several hackle lines (dotted arrows) suggesting a centrifugal direction of crack propagation. Twist hackles are present at the margin of the implant (arrows); these are hackles that separate portions of the cracked surface. Compression curl (CC) is evident at one side suggesting fracture origin at the opposite side. (b) The matching piece of the fractured surface shown in (a), but with titanium abutment screw (TS) at the center which was securing the loaded crown. The fractographic marks observed in (a), such as hackles (dotted arrows) and twist hackle lines (arrows) are reflected on the matching surface. (c) Magnification of a dotted rectangular area near a hackle line depicts one defect (pointer) further magnified in (d).

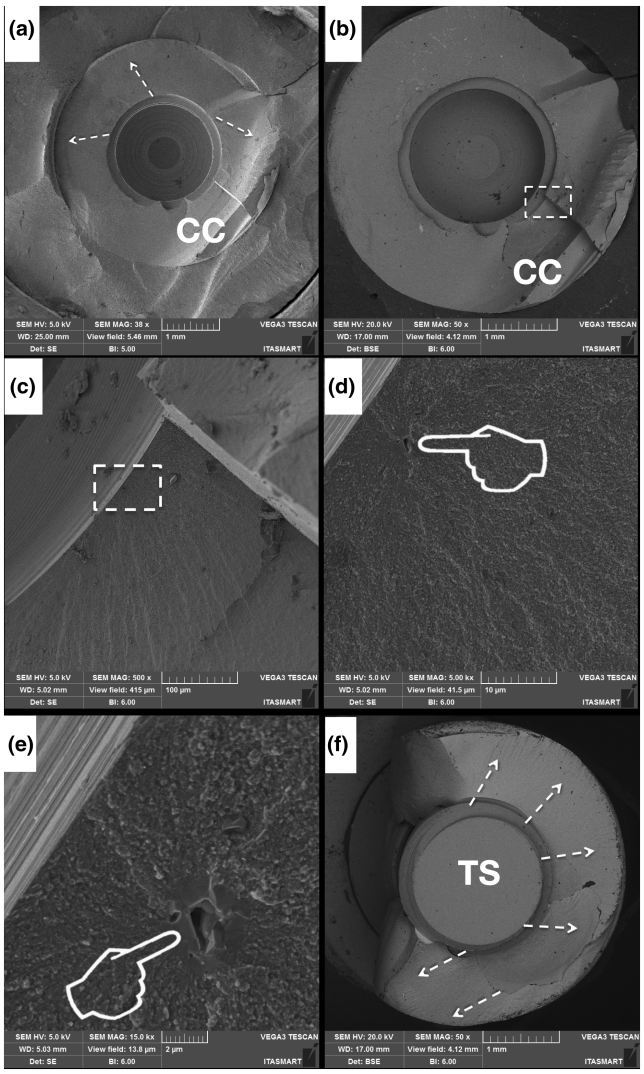

FIGURE 10 Representative SEM micrographs of a fractured zirconia implant with angulated-screw-channel titanium base (Group CI-25—same specimen as in Figure 4). (a) Overview of fractured implant where hackle lines (dotted arrows) suggest the direction of crack propagation, also seen in (b) in backscattered mode. Compression curl indicates that tensile stresses were present at the opposite side, probably at the location of fracture origin. The dotted rectangle magnified in (c) shows its location near the implant-abutment interface where magnification in (d) and (e) depicts a defect (pointer). (f) The matching fractured piece with titanium abutment screw (TS) and hackle lines (dotted arrows) reflecting the direction of crack propagation towards the margins of the ceramic implant.

titanium–zirconium implants and 650 N for two-piece zirconia implants (Hanes et al., 2022). The implants in that investigation were from the same manufacturer as in the present study, restored with anatomical incisor crowns, loaded in a 30° angle, embedded with a 3 mm recession according to ISO 14801, and aged at 37°C for 90 days in an incubator. However, thermomechanical fatigue protocol was not applied, and a longer titanium base (5.5 mm) was used (Hanes et al., 2022). Unfortunately, bending moments or individual lever arms for calculating the bending moments have not been reported to allow for direct comparison.

A similar study investigated both incisor- and molar-shaped screw-retained monolithic zirconia crowns supported by either Ti–Zr or two-piece zirconia implants artificially aged in a chewing simulator (1.2 million cycles, 50 N, 1 Hz) (Joos et al., 2020). The recorded complications and failures are highly dependent on the simulated jaw position. Ti–Zr implants showed higher reliability in the anterior region, whereas zirconia implants showed fewer events in the molar region. None of the anterior two-piece zirconia implants survived aging (0% survival rate), and the complications during thermomechanical loading included implant and screw fractures, and crown loosening or fracture (Joos et al., 2020).

Another in-vitro study reported lower bending moments of 173.7 ± 20.1 N cm for Ti–Zr implants and 171.1 ± 46.1 N cm for two-piece zirconia implants from the same manufacturer (Cantarella et al., 2021). Implants were embedded according to ISO 14801 (30° angle, 3 mm bony recession), restored with anatomical incisor crowns (straight titanium base, short height 3.5 mm), and fatigued using a chewing simulator (1.2 million cycles, 49 N, 1.67 Hz). The

recorded survival rates for Ti–Zr implants were 100% and 83.3% (10/12) for two-piece ceramic implants with two serious abutment failures after thermomechanical loading (Cantarella et al., 2021). Non-serious events included screw loosening in 58.3% (7/12) of the Ti–Zr implants and 10% (1/10) of the ceramic implants, which could be retightened before fracture testing. The authors attributed the higher mechanical stability at the screw level of the zirconia implant compared to that of the titanium implant to the reduced horizontal joint component with an internal connection. The fractures observed after static loading occurred solely at the crown level. Therefore, in that investigation, the weakest link was the all-ceramic lithium disilicate crown leading to lower bending moments and fractures at the level of the crown, compared to the present study, where implants were restored with monolithic zirconia crowns, leading to failures at the implant level and higher bending moment values. The specimens in the present study were free of complications after thermodynamic loading and screw loosening did not occur. Retightening after 10 min may have positively influenced and decreased the complication rate of screw loosening for both SSC and ASC titanium bases on Ti–Zr and zirconia implants in this study (Farina et al., 2014; Spazzin et al., 2010). The fact that ASC titanium bases on ceramic implants might exert a lower preload on the abutment screw due to angulation, leading to lower retaining forces, was not reflected in our results. A laboratory study compared torque differences between SSC and ASC implant crowns on titanium implants before and after simulated functional loading (Swamidass et al., 2021). Differences were not observed between the groups. However, on application of torque values lower than those recommended by the manufacturer, the ASC implant crowns showed a higher percentage of torque differences between the initial and final screw torque values after cyclic loading (Swamidass et al., 2021). Accordingly, the manufacturer's specifications should be observed carefully.

Based on a systematic review, the mechanical threshold for bending moments of ceramic implants should be no less than 200 N cm to ensure clinical safety (Bethke et al., 2020). This threshold value results from the fact that the highest measured bending moment of implants in humans is 95 N cm, and if a 100% safety buffer is added, zirconia implants should have a fatigue strength of at least 200 N cm for clinical applications (Bethke et al., 2020; Morneburg & Pröschel, 2003). The investigated two-piece zirconia implant exceeded this threshold with mean bending moments of 326 N cm for SSC and 434 N cm for ASC titanium bases by far.

Failure analysis revealed different results for the Ti–Zr and CI groups. All specimens of the Ti–Zr groups showed plastic deformation at the abutment and implant levels, while 75% (12/16) of the zirconia implants fractured seriously during single load-to-failure testing at the level of the implant. This might be attributed to the difference in material properties, as titanium shows improved bending and flexural resistance, leading to plastic deformation, whereas zirconia resists greater compressive stress, leading to fracture (Piconi & Maccauro, 1999). Moreover, the observed failure modes suggest that, especially in the presence of excessive and eccentric masticatory forces (e.g., as seen in bruxers), ceramic implants are more likely to cause catastrophic failures compared to titanium implants and may consequently need surgical intervention. In-depth fractographic SEM analysis of ceramic implants revealed important markings, including compressive curls and hackle lines, which indicated that the origin of the failure started from the loading site (Zhang et al., 2020). Fractures occurred either just below the prosthetic screw tip and embedding material, or in combination with a longitudinal fracture of the implant neck on the compression side of the implant, exposing the abutment screw. This fracture pattern indicates that the implant abutment connection might be the weakest link in this system, owing to the reduced wall thickness around the screw (Kohal et al., 2023). Similar fracture schemes have been observed in other two-piece ceramic implant systems (Kohal et al., 2023; Zhang et al., 2020; Zhang, Monzavi, et al., 2022). The observed fracture patterns may have clinical relevance, particularly in peri-implant-infected implants with reduced bony support in the crestal region. In this scenario, the implant abutment connection is exposed to increased stress, particularly under eccentric forces, which may lead to mechanical failure. Remarkably, high load-to-failure values beyond the physiological maximum bite force and implant survival during fatigue could also be correlated with the presence of compressive residual stresses observed in the Raman spectra. In addition, discrete monoclinic peaks were observed in the cervical collar and thread regions.

One limitation of this in-vitro study is the deviation from the ISO standard. However, the present test setup might be closer to observed clinical conditions; the reported bending moments allow comparison with other studies. In addition, an extended chewing simulation with up to 10 million cycles can lead to failure during fatigue.

To the best of our knowledge, this is the first study to investigate the mechanical performance of ASC on two-piece ceramic implants using in-depth fractographic analysis. From a mechanical perspective, the key discoveries of the present study indicate that titanium bases with ASC and ceramic implants are at least equal or even superior in performance to SSC titanium bases and titanium–zirconium implants.

Therefore, ASC allows two-piece ceramic implants to be less invasive in the esthetic zone and permits screw-retained reconstruction in a greater number of clinical cases.

Future and current research avenues in the field of ceramic implantology should explore bone-level two-piece zirconia implants as well as those with a reduced diameter, taper, and short height (<8 mm) (Burkhardt et al., 2021). The next generation of ceramic implants has the potential to allow for a wider range of clinical indications and is expected to gain greater popularity among patients and clinicians.

5 | CONCLUSION

Within the limitations of this in-vitro study, ASC titanium bases and ceramic implants showed significantly higher mean failure load values and bending moments than SSC titanium bases

and titanium–zirconium implants. Both ceramic and titanium–zirconium implants showed high reliability after aging and were free of complications, with a 100% survival rate. However, most ceramic implants exhibit severe fractures after single load-to-failure testing, whereas titanium implant failures are restricted to plastic deformation.

Therefore, from a mechanical perspective, titanium bases with ASCs appear to be as reliable as SSC titanium bases for ceramic and titanium implants. The tested two-piece zirconia implant, with its prefabricated SSC and ASC titanium base, seem suitable for clinical applications and can withstand high failure loads. Prospective clinical studies are required to corroborate the results of the present study.

AUTHOR CONTRIBUTIONS

E. Helal: Data curation; Visualization; Investigation; Writing—original draft; Formal analysis. **P. C. Gierthmuehlen:** Resources; Project administration; Funding acquisition; Writing—review and editing; Conceptualization; Validation; Supervision. **E. A. Bonfante:** Writing—review and editing; Validation; Formal analysis; Data curation. **T. M. B. Campos:** Visualization; Writing—review and editing; Data curation. **L. S. Prott:** Writing—review and editing; Data curation; Formal analysis. **R. Langner:** Writing—review and editing; Visualization; Formal analysis; Software. **F. A. Spitznagel:** Supervision; Conceptualization; Writing—original draft; Data curation; Investigation; Project administration; Funding acquisition; Formal analysis; Methodology.

ACKNOWLEDGMENTS

The authors would like to thank MDT Boris Martin for the fabrication of the implant crowns and Dr. Aimen Bagegni for his advice during the pretests of the study. Part of this publication was required for E. Helal to fulfill his Dr. med. dent. degree. Open Access funding enabled and organized by Projekt DEAL.

FUNDING INFORMATION

This research did not receive any specific grant from funding agencies in the public, commercial or non-profit sectors. The implants and abutments were kindly provided by Institut Straumann AG (Basel, Switzerland).

CONFLICT OF INTEREST STATEMENT

The authors declare no conflict of interest.

DATA AVAILABILITY STATEMENT

The datasets from this study are available from the corresponding author upon reasonable request.

ORCID

P. C. Gierthmuehlen https://orcid.org/0000-0002-4837-2546
E. A. Bonfante https://orcid.org/0000-0001-6867-8350
L. S. Prott https://orcid.org/0000-0003-0792-0830
R. Langner https://orcid.org/0000-0002-3237-001X
F. A. Spitznagel https://orcid.org/0000-0001-5535-2108

REFERENCES

Alves, L. M. M., da Silva Rodrigues, C., Ramos, G. F., Campos, T. M. B., & de Melo, R. M. (2022). Wear behavior of silica-infiltrated monolithic zirconia: Effects on the mechanical properties and surface characterization. *Ceramics International*, *48*(5), 6649–6656.

Balmer, M., Payer, M., Kohal, R. J., & Spies, B. C. (2022). EAO position paper: Current level of evidence regarding zirconia implants in clinical trials. *The International Journal of Prosthodontics*, *35*(4), 560–566. https://doi.org/10.11607/ijp.8131

Bethke, A., Pieralli, S., Kohal, R. J., Burkhardt, F., von Stein-Lausnitz, M., Vach, K., & Spies, B. C. (2020). Fracture resistance of zirconia oral implants in vitro: A systematic review and meta-analysis. *Materials (Basel)*, *13*(3), 562. https://doi.org/10.3390/ma13030562

Bienz, S. P., Hilbe, M., Hüsler, J., Thoma, D. S., Hämmerle, C. H. F., & Jung, R. E. (2021). Clinical and histological comparison of the soft tissue morphology between zirconia and titanium dental implants under healthy and experimental mucositis conditions—A randomized controlled clinical trial. *Journal of Clinical Periodontology*, *48*(5), 721–733. https://doi.org/10.1111/jcpe.13411

Bonfante, E. A., & Coelho, P. G. (2016). A critical perspective on mechanical testing of implants and prostheses. *Advances in Dental Research*, *28*(1), 18–27. https://doi.org/10.1177/0022034515624445

Burkhardt, F., Spies, B. C., Riemer, L., Adolfsson, E., Doerken, S., & Kohal, R. J. (2021). Fracture resistance and crystal phase transformation of a one- and a two-piece zirconia implant with and without simultaneous loading and aging—An in vitro study. *Clinical Oral Implants Research*, *32*(11), 1288–1298. https://doi.org/10.1111/clr.13825

Buser, D., Martin, W., & Belser, U. C. (2004). Optimizing esthetics for implant restorations in the anterior maxilla: Anatomic and surgical considerations. *The International Journal of Oral & Maxillofacial Implants*, *19*(Suppl), 43–61.

Cantarella, J., Pitta, J., Mojon, P., Hicklin, S. P., Fehmer, V., & Sailer, I. (2021). Mechanical stability of restorations supported by titanium base, zirconia, and polyetherketoneketone abutments on one- and two-piece zirconia implants. *The International Journal of Oral & Maxillofacial Implants*, *36*(2), 313–321. https://doi.org/10.11607/jomi.8798

Chappuis, V., Engel, O., Reyes, M., Shahim, K., Nolte, L. P., & Buser, D. (2013). Ridge alterations post-extraction in the esthetic zone: A 3D analysis with CBCT. *Journal of Dental Research*, *92*(12 Suppl), 195S–201S. https://doi.org/10.1177/0022034513506713

Chen, S. T., Buser, D., Sculean, A., & Belser, U. C. (2023). Complications and treatment errors in implant positioning in the aesthetic zone: Diagnosis and possible solutions. *Periodontology 2000*. https://doi.org/10.1111/prd.12474

Cionca, N., Hashim, D., & Mombelli, A. (2017). Zirconia dental implants: Where are we now, and where are we heading? *Periodontology 2000*, *73*(1), 241–258. https://doi.org/10.1111/prd.12180

Delong, R., Sakaguchi, R. L., Douglas, W. H., & Pintado, M. R. (1985). The wear of dental amlgam in an artifical mouth: A clinical correlation. *Dental Materials*, *1*, 238–242. https://doi.org/10.1016/S0109-5641(85)80050-6

Di Fiore, A., Granata, S., Monaco, C., Stellini, E., & Yilmaz, B. (2023). Clinical performance of posterior monolithic zirconia implant-supported fixed dental prostheses with angulated screw channels: A 3-year prospective cohort study. *The Journal of Prosthetic Dentistry*, *129*, 566–572. https://doi.org/10.1016/j.prosdent.2021.06.043

Edmondson, E. K., Trejo, P. M., Soldatos, N., & Weltman, R. L. (2022). The ability to screw-retain single implant-supported restorations in the anterior maxilla: A CBCT analysis. *The Journal of Prosthetic Dentistry*, *128*(3), 443–449. https://doi.org/10.1016/j.prosdent.2021.01.004

Farina, A. P., Spazzin, A. O., Consani, R. L., & Mesquita, M. F. (2014). Screw joint stability after the application of retorque in implant-supported

dentures under simulated masticatory conditions. *The Journal of Prosthetic Dentistry*, *111*(6), 499–504. https://doi.org/10.1016/j.prosdent.2013.07.024

Gahlert, M., Kniha, H., Laval, S., Gellrich, N. C., & Bormann, K. H. (2022). Prospective clinical multicenter study evaluating the 5-year performance of zirconia implants in single-tooth gaps. *The International Journal of Oral & Maxillofacial Implants*, *37*(4), 804–811. https://doi.org/10.11607/jomi.9289

Garcia-Gazaui, S., Razzoog, M., Sierraalta, M., & Saglik, B. (2015). Fabrication of a screw-retained restoration avoiding the facial access hole: A clinical report. *The Journal of Prosthetic Dentistry*, *114*(5), 621–624. https://doi.org/10.1016/j.prosdent.2015.06.007

Hanes, B., Feitosa, S., Phasuk, K., Levon, J. A., Morton, D., & Lin, W. S. (2022). Fracture resistance behaviors of titanium–zirconium and zirconia implants. *Journal of Prosthodontics*, *31*(5), 441–446. https://doi.org/10.1111/jopr.13440

Hein, D., Joly, J. C., Napimoga, M. H., Peruzzo, D. C., & Martinez, E. F. (2021). Influence of abutment angulation on loss of prosthetic abutment torque under mechanical cycling. *The Journal of Prosthetic Dentistry*, *125*(2), 349.e341–e346. https://doi.org/10.1016/j.prosdent.2020.10.010

Hotinski, E., & Dudley, J. (2019). Abutment screw loosening in angulation-correcting implants: An in vitro study. *The Journal of Prosthetic Dentistry*, *121*(1), 151–155. https://doi.org/10.1016/j.prosdent.2018.03.005

ISO 14801. (2016). Dentistry—Implants—Dynamic loading test for endosseous dental implants. *ISO 14801*, *2016*(E), 1–22.

Janner, S. F. M., Gahlert, M., Bosshardt, D. D., Roehling, S., Milz, S., Higginbottom, F., Buser, D., & Cochran, D. L. (2018). Bone response to functionally loaded, two-piece zirconia implants: A preclinical histometric study. *Clinical Oral Implants Research*, *29*(3), 277–289. https://doi.org/10.1111/clr.13112

Joos, M., Sailer, I., Filippi, A., Mukaddam, K., Rosentritt, M., & Kühl, S. (2020). Stability of screw-retention in two-piece zirconia implants: An in vitro study. *Clinical Oral Implants Research*, *31*, 607–614. https://doi.org/10.1111/clr.13597

Kern, M., Strub, J. R., & Lü, X. Y. (1999). Wear of composite resin veneering materials in a dual-axis chewing simulator. *Journal of Oral Rehabilitation*, *26*(5), 372–378. https://doi.org/10.1046/j.1365-2842.1999.00416.x

Kniha, K., Kniha, H., Grunert, I., Edelhoff, D., Hölzle, F., & Modabber, A. (2019). Esthetic evaluation of maxillary single-tooth zirconia implants in the esthetic zone. *The International Journal of Periodontics & Restorative Dentistry*, *39*(5), e195–e201. https://doi.org/10.11607/prd.3282

Kohal, R. J., Spies, B. C., Vach, K., Balmer, M., & Pieralli, S. (2020). A prospective clinical cohort investigation on zirconia implants: 5-year results. *Journal of Clinical Medicine*, *9*(8), 2585. https://doi.org/10.3390/jcm9082585

Kohal, R. J., von Schierholz, C., Nold, J., Spies, B. C., Adolfsson, E., Vach, K., & Burkhardt, F. (2023). Influence of loading and aging on the fracture strength of an injection-molded two-piece zirconia implant restored with a zirconia abutment. *Clinical Oral Implants Research*, *34*(2), 105–115. https://doi.org/10.1111/clr.14022

Korkmaz, I. H., & Kul, E. (2022). Investigation of the type of angled abutment for anterior maxillary implants: A finite element analysis. *Journal of Prosthodontics*, *31*(8), 689–696. https://doi.org/10.1111/jopr.13462

Lorenz, J., Parvini, P., Obreja, K., Trimpou, G., Linder, S., Hölscher, W., Dard, M., Schwarz, F., & Sader, R. (2022). Clinical performance of a newly developed two-piece zirconia implant system in the maxilla: A prospective multicentre study. *International Journal of Oral Implantology*, *15*(4), 327–338.

Lv, X. L., Qian, S. J., Qiao, S. C., Gu, Y. X., Lai, H. C., & Shi, J. Y. (2021). Clinical, radiographic, and immunological evaluation of angulated screw-retained and cemented single-implant crowns in the esthetic region: A 1-year randomized controlled clinical trial. *Clinical Implant Dentistry and Related Research*, *23*(5), 692–702. https://doi.org/10.1111/cid.13035

Morneburg, T. R., & Pröschel, P. A. (2003). In vivo forces on implants influenced by occlusal scheme and food consistency. *The International Journal of Prosthodontics*, *16*(5), 481–486.

Nishihara, H., Haro Adanez, M., & Att, W. (2019). Current status of zirconia implants in dentistry: Preclinical tests. *Journal of Prosthodontic Research*, *63*(1), 1–14. https://doi.org/10.1016/j.jpor.2018.07.006

Opler, R., Wadhwani, C., & Chung, K. H. (2020). The effect of screwdriver angle variation on the off-axis implant abutment system and hexalobular screw. *The Journal of Prosthetic Dentistry*, *123*(3), 524–528. https://doi.org/10.1016/j.prosdent.2019.01.008

Piconi, C., & Maccauro, G. (1999). Zirconia as a ceramic biomaterial. *Biomaterials*, *20*(1), 1–25.

Pieralli, S., Kohal, R. J., Jung, R. E., Vach, K., & Spies, B. C. (2017). Clinical outcomes of zirconia dental implants: A systematic review. *Journal of Dental Research*, *96*(1), 38–46. https://doi.org/10.1177/0022034516664043

Pitman, J., van Craenenbroeck, M., Glibert, M., & Christiaens, V. (2022). Screw loosening in angulation-correcting single implant restorations: A systematic review of in vitro studies. *The Journal of Prosthetic Dentistry*. https://doi.org/10.1016/j.prosdent.2022.08.003

Prado, P., Monteiro, J. B., Campos, T. M. B., Thim, G. P., & de Melo, R. M. (2020). Degradation kinetics of high-translucency dental zirconias: Mechanical properties and in-depth analysis of phase transformation. *Journal of the Mechanical Behavior of Biomedical Materials*, *102*, 103482. https://doi.org/10.1016/j.jmbbm.2019.103482

Ramos, N. C., Kaizer, M. R., Campos, T. M. B., Kim, J., Zhang, Y., & Melo, R. M. (2019). Silica-based infiltrations for enhanced zirconia-resin interface toughness. *Journal of Dental Research*, *98*(4), 423–429. https://doi.org/10.1177/0022034518819477

Rella, E., de Angelis, P., Damis, G., D'Addona, A., & Manicone, P. F. (2021). The application of angulated screw-channels in metal-free, implant-supported restorations: A retrospective survival analysis. *Materials (Basel)*, *14*(22), 7006. https://doi.org/10.3390/ma14227006

Righetti, V., Campos, T., Robatto, L., Rego, R., & Thim, G. (2020). Non-destructive surface residual stress profiling by multireflection grazing incidence X-ray diffraction: A 7050 Al alloy study. *Experimental Mechanics*, *60*, 475–480.

Roehling, S., Schlegel, K. A., Woelfler, H., & Gahlert, M. (2018). Performance and outcome of zirconia dental implants in clinical studies: A meta-analysis. *Clinical Oral Implants Research*, *29*(Suppl 16), 135–153. https://doi.org/10.1111/clr.13352

Roehling, S., Schlegel, K. A., Woelfler, H., & Gahlert, M. (2019). Zirconia compared to titanium dental implants in preclinical studies—A systematic review and meta-analysis. *Clinical Oral Implants Research*, *30*(5), 365–395. https://doi.org/10.1111/clr.13425

Rosentritt, M., Behr, M., van der Zel, J. M., & Feilzer, A. J. (2009). Approach for valuating the influence of laboratory simulation. *Dental Materials*, *25*(3), 348–352. https://doi.org/10.1016/j.dental.2008.08.009

Sailer, I., Karasan, D., Todorovic, A., Ligoutsikou, M., & Pjetursson, B. E. (2022). Prosthetic failures in dental implant therapy. *Periodontology 2000*, *88*(1), 130–144. https://doi.org/10.1111/prd.12416

Spazzin, A. O., Henrique, G. E., Nobilo, M. A., Consani, R. L., Correr-Sobrinho, L., & Mesquita, M. F. (2010). Effect of retorque on loosening torque of prosthetic screws under two levels of fit of implant-supported dentures. *Brazilian Dental Journal*, *21*(1), 12–17. https://doi.org/10.1590/s0103-64402010000100002

Spies, B. C., Nold, J., Vach, K., & Kohal, R. J. (2016). Two-piece zirconia oral implants withstand masticatory loads: An investigation in the artificial mouth. *Journal of the Mechanical Behavior of Biomedical Materials*, *53*, 1–10. https://doi.org/10.1016/j.jmbbm.2015.07.005

Spitznagel, F. A., Balmer, M., Wiedemeier, D. B., Jung, R. E., & Gierthmuehlen, P. C. (2022). Clinical outcomes of all-ceramic single crowns and fixed dental prostheses supported by ceramic implants: A systematic review and meta-analyses. *Clinical Oral Implants Research*, *33*(1), 1–20. https://doi.org/10.1111/clr.13871

Staubli, N., Walter, C., Schmidt, J. C., Weiger, R., & Zitzmann, N. U. (2017). Excess cement and the risk of peri-implant disease—A systematic review. *Clinical Oral Implants Research*, *28*(10), 1278–1290. https://doi.org/10.1111/clr.12954

Swamidass, R. S., Kan, J. Y. K., Kattadiyil, M. T., Goodacre, C. J., & Lozada, J. (2021). Abutment screw torque changes with straight and angled screw-access channels. *The Journal of Prosthetic Dentistry*, *125*(4), 675–681. https://doi.org/10.1016/j.prosdent.2020.01.018

Tanaka, M., Kitazawa, R., Tomimatsu, T., Liu, Y., & Kagawa, Y. (2009). Residual stress measurement of an EB-PVD Y_2O_3–ZrO_2 thermal barrier coating by micro-Raman spectroscopy. *Surface and Coatings Technology*, *204*(5), 657–660.

Thoma, D. S., Benic, G. I., Munoz, F., Kohal, R., Sanz Martin, I., Cantalapiedra, A. G., Hämmerle, C. H., & Jung, R. E. (2015). Histological analysis of loaded zirconia and titanium dental implants: An experimental study in the dog mandible. *Journal of Clinical Periodontology*, *42*(10), 967–975. https://doi.org/10.1111/jcpe.12453

Wilson, T. G., Jr. (2009). The positive relationship between excess cement and peri-implant disease: A prospective clinical endoscopic study. *Journal of Periodontology*, *80*(9), 1388–1392. https://doi.org/10.1902/jop.2009.090115

Zhang, F., Meyer Zur Heide, C., Chevalier, J., Vleugels, J., van Meerbeek, B., Wesemann, C., Camargo Dos Santos, B., Sergo, V., Kohal, R. J., Adolfsson, E., Herklotz, I., & Spies, B. C. (2020). Reliability of an injection-moulded two-piece zirconia implant with PEKK abutment after long-term thermo-mechanical loading. *Journal of the Mechanical Behavior of Biomedical Materials*, *110*, 103967. https://doi.org/10.1016/j.jmbbm.2020.103967

Zhang, F., Monzavi, M., Li, M., Cokic, S., Manesh, A., Nowzari, H., Vleugels, J., & van Meerbeek, B. (2022). Fracture analysis of one/two-piece clinically failed zirconia dental implants. *Dental Materials*, *38*(10), 1633–1647. https://doi.org/10.1016/j.dental.2022.08.004

Zhang, Y., Yu, P., & Yu, H. (2022). Stress distribution and microgap formation in angulated zirconia abutments with a titanium base in narrow diameter implants: A 3D finite element analysis. *International Journal for Numerical Methods in Biomedical Engineering*, *38*(7), e3610. https://doi.org/10.1002/cnm.3610

How to cite this article: Helal, E., Gierthmuehlen, P. C., Bonfante, E. A., Campos, T. M. B., Prott, L. S., Langner, R., & Spitznagel, F. A. (2023). Influence of straight versus angulated screw channel titanium bases on failure loads of two-piece ceramic and titanium implants restored with screw-retained monolithic crowns: An in-vitro study. *Clinical Oral Implants Research*, *34*, 1217–1229. https://doi.org/10.1111/clr.14157